only some of them will be chosen to stay in the last step. The process to select potential edges by setting two thresholds is called double thresholding.

The last step in the edge detection of canny edge detection involve suppressing all edges that are not connected to strong or true edges. The weak edges found in previous step can only be preserved to the final edge image if they are connected to the true edges. The reason for this step is to remove the weak edges that are caused by noises or other small variations. This process of selecting true edges from weak edges is named as hysteresis. The steps started from SRAD until hysteresis is summarized in the following flow chart.

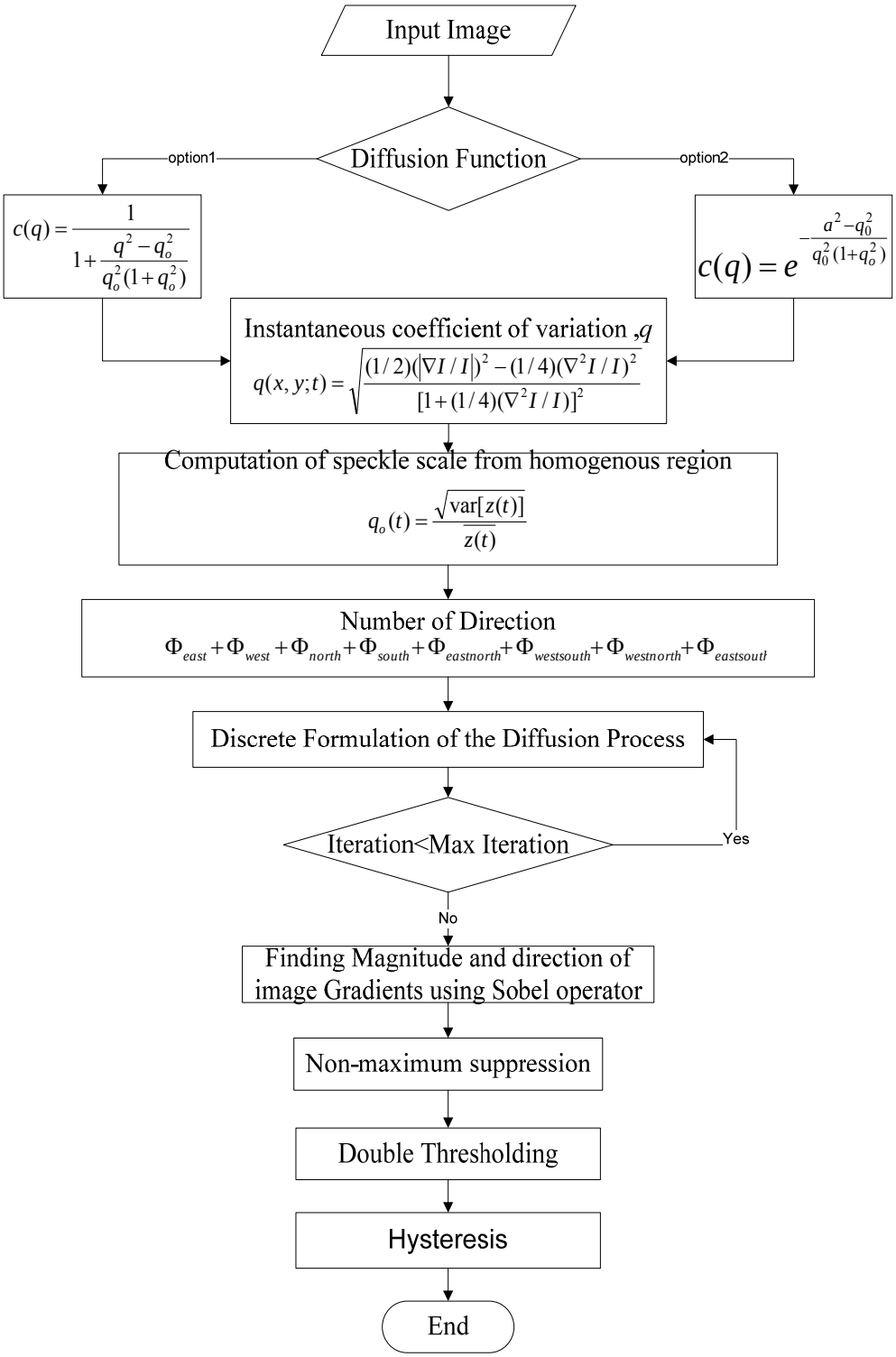

Fig.1 Flow chart of the methodology for the proposed edge detection

3 Results

In this section, the ultrasound phantom in figure 2.0 will undergo conventional canny edge detection and the proposed method edge detection at different thresholds and different standard deviation separately and the result is shown in figure 3.0 and figure 4.0.

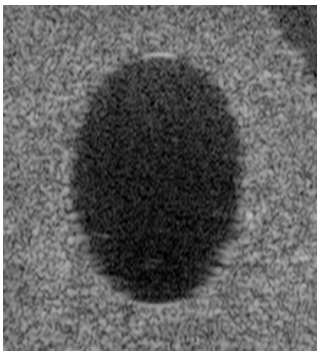

Fig. 2 Original ultrasound phantoms Image

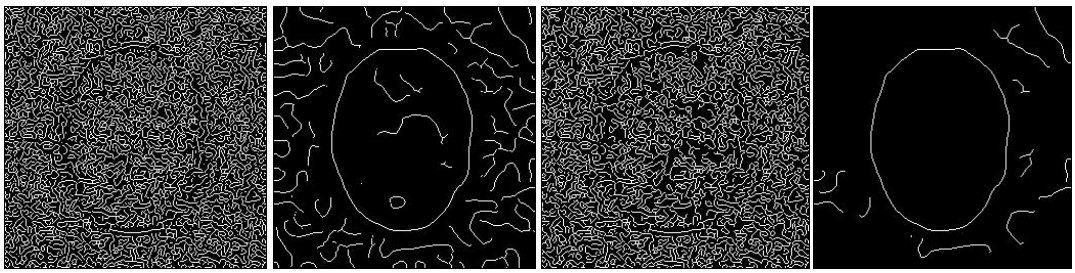

(a)Threshold=0.04,0.1 (b) Threshold=0.08,0.2

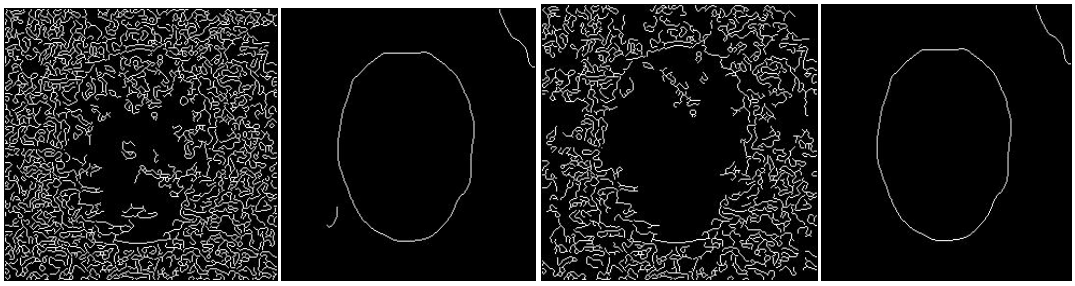

(c)Threshold=0.12,0.3 (d) Threshold=0.16,0.4

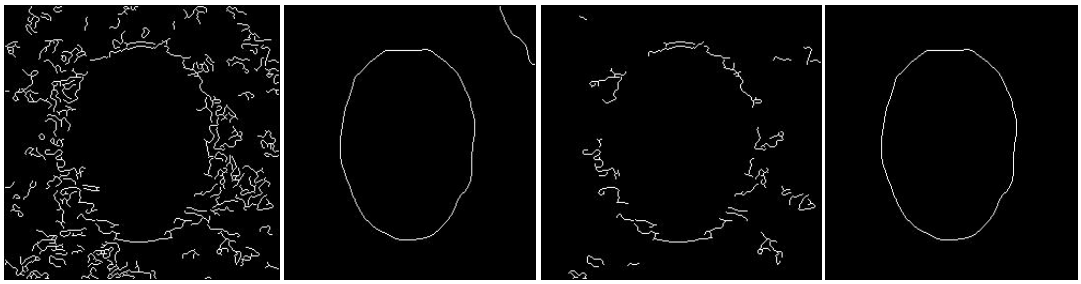

(e) Threshold=0.20,0.5 (f) Threshold=0.24,0.6

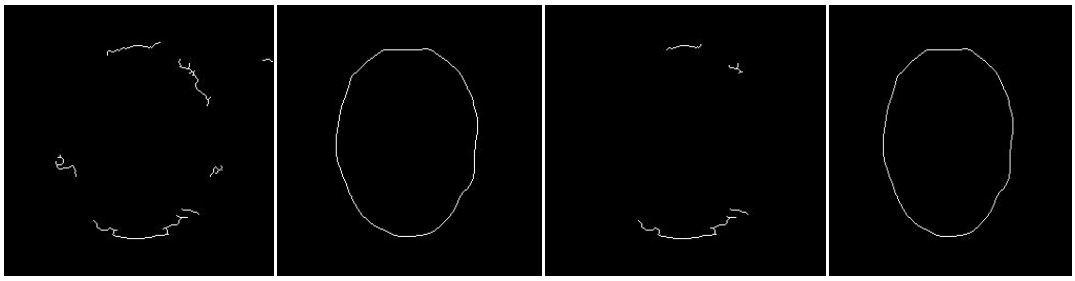

(g) Threshold=0.28,0.7 (h)Threshold=0.32,0.8

Fig. 3 Comparison between conventional canny edge detector and SRAD-Canny edge detector on noisy image of ultrasound with standard deviation of 1.0. The first and third columns are the image result by conventional canny detector. The second and fourth columns are the SRAD-Canny edge detector result image.

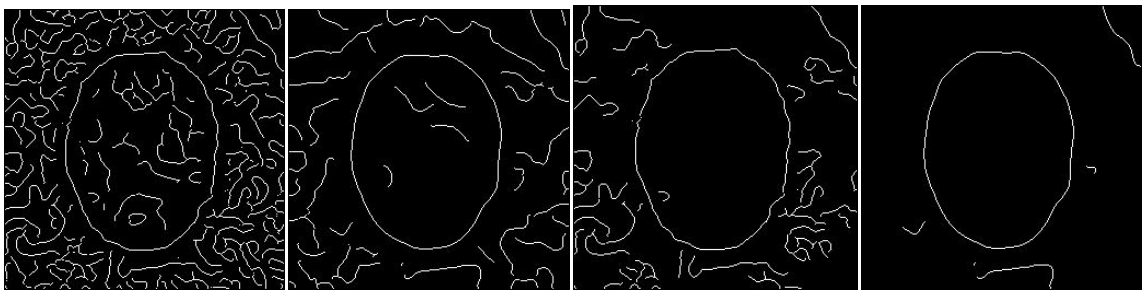

(a) Threshold=0.04,0.1 (b) Threshold=0.08,0.2

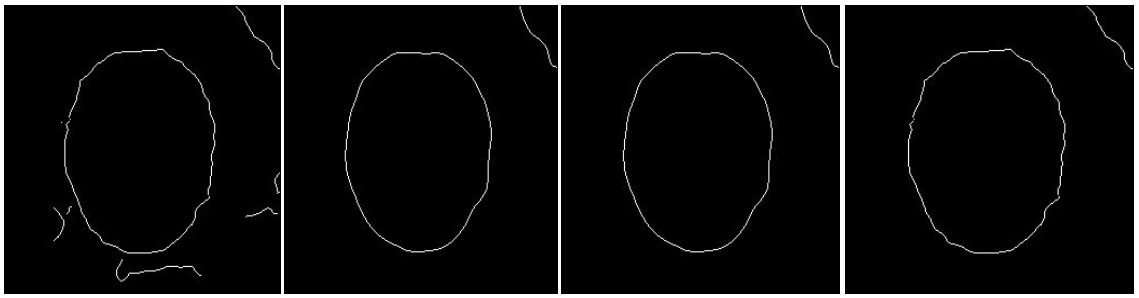

(c) Threshold=0.12,0.3 (d) Threshold=0.16,0.4

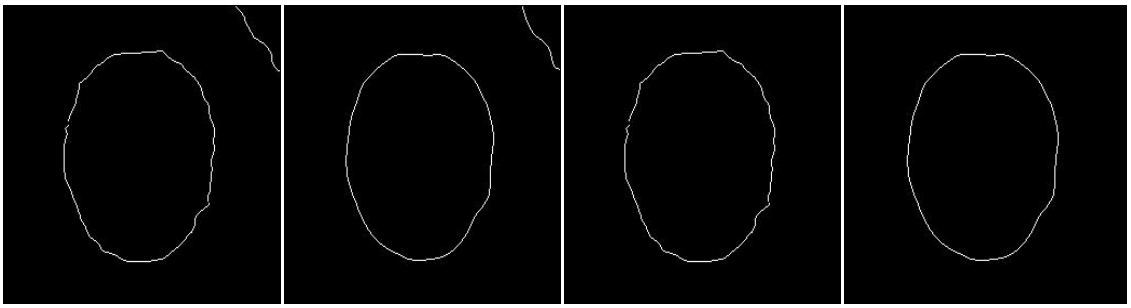

(e) Threshold=0.2,0.5 (f) Threshold=0.24,0.6

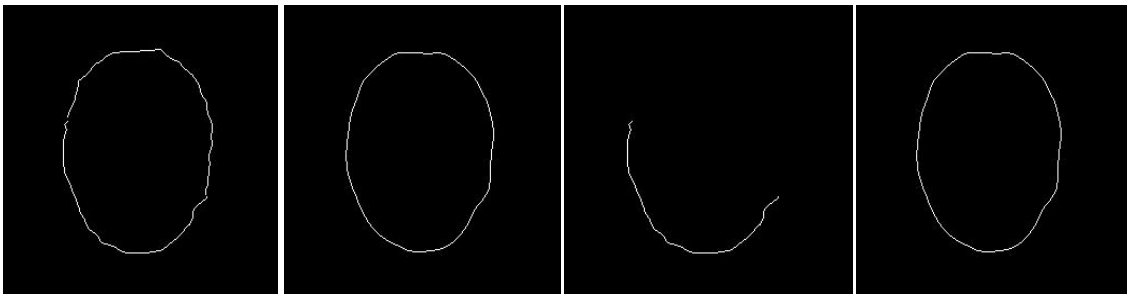

(g) Threshold=0.28,0.7 (h) Threshold=0.32,0.8

Fig. 4 Comparison between conventional canny edge detector and SRAD-Canny edge detector on noisy image of ultrasound with standard deviation of 3.0. The first and third columns are the image result by conventional canny detector. The second and fourth columns are the SRAD-Canny edge detector result image

4 Discussion

From figure 1, it can be observed that at threshold value of 0.1, the image generated from conventionally canny using Gaussian blurring result in a noisy result whereas the image generated using SRAD-Canny Edge detector shows less noisy result with the elliptical shape object observable. At threshold value of 0.2, 0.3 and 0.4, the conventional canny detector result remains a noisy image although the middle of the elliptical shape begin to appear whereas the SRAD-canny edge result in a clear and clean edge of the elliptic shape. At threshold 0.5, 0.6, 0.7, 0.8, the conventional canny detector result in less noisy edge around elliptic shape, however the strong edge of the elliptic shape is reduced as well, and the shape is not observable whereas the SRAD-canny is obviously presenting a complete shape of ellipse and free of noisy edges.

From figure 2, the edge detection is carried out in higher value of standard deviation of Gaussian blurring, at threshold of 0.1, 0.2, 0.3, the result image of conventional canny edge detector contains more noisy edges than SRAD-canny edge detector. At threshold of 0.4, 0.5, 0.6, 0.7, the elliptic shape is obtained for conventional canny edge, however, the shape is not complete, it can be found that small hole appears inside the shape. At higher value of threshold, the shape disappears and left a fraction of the edge. Through subjective evaluation, result shows that the conventional method is only capable of producing promising result if the parameter is correctly set. The proposed method, in contrast, can produce promising result in a very wider range of parameter values.

4.1 Quantitative analysis on the result

$$PSNR = 10\log_{10}\left(\frac{G_{\max}^2}{\sum_i^M \sum_j^N (I(i,j) - I^*(i,j))^2}\right) \tag{9}$$

Denotation: Where $G_{\max}$ is the maximum gray level of the image. where $I^*(i,j)$ represents pixel intensity in ith row and jth column processed image and $I(i,j)$ represents pixel intensity in ith row and jth column in the original image. M and N depicts maximum number of row and maximum number of column of the image matrix.

$$SNR = 10\log_{10}\left(\frac{\sigma_I^2}{\sigma_{I-I^*}^2}\right) \tag{10}$$

Denotation: where σ^2 denotes the variance of the original image, $\sigma_{I-I^*}^2$ denotes the variance of the smoothed image. The performance of the smoothing algorithm increases with the SNR value.

$$RMSE = \sqrt{\frac{1}{MxN}\sum_{i=1}^M \sum_{j=1}^N (I^*(i,j) - I(i,j))^2} \tag{11}$$

Where $I^*(i,j)$ represents pixel intensity in ith row and jth column processed image and $I(i,j)$ represents pixel intensity in ith row and jth column in the original image. M and N depicts maximum number of row and maximum number of column of the image matrix.The value of RMSE indicates the

total difference of pixel intensity in processed image and original image. Therefore, with larger value of RMSE, it indicates poorer information preservation.

$$FOM = \frac{1}{MAX\{N_a, N_d\}} \sum_{i=1}^{N_a} \frac{1}{1 + d_i^2 e} \quad (12)$$

Where N_r denotes actual edge map points, N_d denotes the ideal edge map points. d is the Euclidean distance difference calculated as actual edge point normal to a line of ideal edge points. The e denotes weighting factor. The *FOM* is equals to unity if the actual edge is perfectly merged with the detected edge. The weighting factor can be adjusted to penalize edges that are localized but deviated from the ideal position.

The result shown in table 1 indicates that the proposed method can produce image that has highest value of PSNR, SNR and RMSE. This implies that the proposed method produce less pixilated image. Besides, the FOM value indicates that the proposed method can detect edge with higher accuracy. All the highest value in the table has been bold for the comparison sake.

Table 1 Performance comparisons for ultrasound phantom image using quantitative analysis

	Quantitative Evaluations			
	PSNR	SNR	RMSE	FOM
Gaussian	13.3253	8.4564	29.4356	0.1356
KUAN[32]	14.3245	8.8976	27.3546	0.2465
AWMF[33]	14.2132	9.4564	26.4337	0.4566
SRAD[29]	16.4654	10.5676	15.4674	0.6342
PMAD[24]	14.6768	9.5468	19.3445	0.5434
PROPOSED	**17.4546**	**12.3556**	**13.7344**	**0.6779**

5 Conclusion

This paper presented an improved Canny edge detector by incorporating it with Speckle reducing anisotropic diffusion method in eight directions which can adapt to ultrasonic local speckle statistic. Experimental results on ultrasound phantom shows that the proposed method can preserve edges and small structures while removing speckle noise effectively at a wide range of threshold and standard deviation. Thus, it has the potential to enhance the diagnostic ultrasound imaging and to improve automated segmentation and edge detection technique. Future efforts should be focus on the thresholding step in Canny edge detection in order to make it become more adaptive to the noisy image.

References:

[1] Tang, H., et al., MRI brain image segmentation by multi-resolution edge detection and region selection. *Computerized Medical Imaging and Graphics*, Vol. 24, No. 6, 2000, pp. 349-357.

[2] Chai, H.Y., et al., GLCM based adaptive crossed reconstructed (ACR) k-mean clustering hand bone segmentation, *in 10th WSEAS international conference on signal processing, robotics and automation.*, 2011 pp. 192-197.

[3] Sauer, K., Enhancement of low bit-rate coded images using edge detection and estimation. *CVGIP: Graphical Models and Image Processing*, Vol. 31, No. 1, 1991, pp. 52-62.

[4] Garlipp, T. and C.H. Müller, Detection of linear and circular shapes in image analysis. *Computational Statistics & Data Analysis*, Vol. 51, No. 3, 2006, pp. 1479-1490.

[5] Chai, H.Y., et al., Adaptive Crossed Reconstructed (ACR) K-mean Clustering Segmentation for Computer-aided Bone Age Assessment System. International Journal of *Mathematical Models and Methods in Applied Sciences*, Vol. 5, No.3, 2011, pp. 628-635.

[6] Román-Roldán, R., et al., A measure of quality for evaluating methods of segmentation and edge detection. *Pattern Recognition*, Vol.34, No.5, 2001, pp. 969-980.

[7] Yu, Y.-H. and C.-C. Chang, A new edge detection approach based on image context analysis. *Image and Vision Computing*, Vol. 24, No.10, 2006, pp. 1090-1102.

[8] Accame, M. and F.G.B. De Natale, Edge detection by point classification of Canny

filtered images. *Signal Processing*, Vol.60, No.1, 1997, pp. 11-22.
[9] Johnson, R.P., Contrast based edge detection. *Pattern Recognition*, Vol.23, No.3, 1990, pp. 311-318.
[10] Chai, H.Y., et al., Gray-level co-occurrence matrix bone fracture detection. *American Journal of Applied Sciences*, Vol.8, No.1, 2011, pp. 26-32.
[11] Clark, J.J., Authenticating edges produced by zero-crossing algorithms. *Pattern Analysis and Machine Intelligence, IEEE Transactions on*, Vol.11, No.1, 1989, pp. 43-57.
[12] Aarnink, R., et al., Edge detection in prostatic ultrasound images using integrated edge maps. *Ultrasonics*, Vol.36, No.1, 1998, pp. 635-642.
[13] Shih, M.-Y. and D.-C. Tseng, A wavelet-based multiresolution edge detection and tracking. *Image and Vision Computing*, Vol.23, No.4, 2005, pp. 441-451.
[14] Gonzalez, R. and R. Woods, Digital Image Processing: Addison-Wesley Longman Publishing Co., Inc., 2001
[15] Roberts, L., Machine perception of three-dimensional solids, Massachusetts Institute of Technology, 1963
[16] Chaudhuri, B.B. and B. Chanda, The equivalence of best plane fit gradient with Robert's, Prewitt's and Sobel's gradient for edge detection and a 4-neighbour gradient with useful properties. *Signal Processing*, Vol.6, No.2, 1984, pp. 143-151.
[17] Mlsna, P.A. and J.J. Rodriguez, Gradient and Laplacian Edge Detection, in Handbook of Image and Video Processing (Second Edition), B. Al, Editor. 2005, Academic Press: Burlington. pp. 535-553.
[18] Rosenfeld, A. and M. Thurston, Edge and Curve Detection for Visual Scene Analysis. *Computers, IEEE Transactions on,* Vol.20, No.5, 1971, pp. 562-569.
[19] Marr, D. and E. Hildreth, Theory of Edge Detection. Proceedings of the Royal Society of London. Series B, *Biological Sciences*, Vol.207, No.1167, 1980. pp. 187-217.
[20] Canny, J., A Computational Approach to Edge Detection. *Pattern Analysis and Machine Intelligence, IEEE Transactions on*, Vol.8, No.6, 1986, pp. 679-698.
[21] Heath, M.D., et al., A robust visual method for assessing the relative performance of edge-detection algorithms. *Pattern Analysis and Machine Intelligence, IEEE Transactions on*, Vol.19, No.12, 1997, pp. 1338-1359.
[22] Medina-Carnicer, R., et al., A novel method to look for the hysteresis thresholds for the Canny edge detector. *Pattern Recognition*, Vol.24, No.6, 2011. pp. 1201-1211.
[23] Hou, Z.J. and G.W. Wei, A new approach to edge detection. *Pattern Recognition*, Vol.35, No.7, 2002. pp. 1559-1570.
[24] Perona, P. and J. Malik, Scale-space and edge detection using anisotropic diffusion. *Pattern Analysis and Machine Intelligence, IEEE Transactions on*, Vol.12, No.7, 1990. pp. 629-639.
[25] Xiaona, Z. and W. Tianfu. An anisotropic diffusion filter for ultrasonic speckle reduction. in Visual Information Engineering, 2008. *VIE 2008. 5th International Conference on*. 2008.
[26] Byeongcheol, Y. and T. Nishimura. A study of ultrasound images enhancement using adaptive speckle reducing anisotropic diffusion. in Industrial Electronics, 2009. ISIE 2009. IEEE International Symposium on. 2009.
[27] Aksel, A., et al. Speckle Reducing Anisotropic Diffusion for Echocardiography. in Signals, Systems and Computers, 2006. ACSSC '06. Fortieth Asilomar Conference on. 2006.
[28] Yoo, B.C., et al. Multi-scale Based Adaptive SRAD for Ultrasound Images Enhancement. in World Congress on Engineering and Computer Science 2008, WCECS '08. Advances in Electrical and Electronics Engineering - IAENG Special Edition of the. 2008.
[29] Yongjian, Y. and S.T. Acton, Speckle reducing anisotropic diffusion. *Image Processing, IEEE Transactions on*, Vol.11, No.11, 2002. pp. 1260-1270.
[30] Liu, G., et al., Speckle reduction by adaptive window anisotropic diffusion. *Signal Processing*, Vol.89, No.11, 2009. pp. 2233-2243.
[31] Gerig, G., et al., Nonlinear anisotropic filtering of MRI data. *Medical Imaging, IEEE Transactions on*, Vol.11, No.2, 1992. pp. 221-232.
[32] Kuan, D., et al., Adaptive restoration of images with speckle. Acoustics, *Speech and Signal Processing, IEEE Transactions on*, Vol.35, No.3, 1987. pp. 373-383.
[33] Loupas, T., W.N. McDicken, and P.L. Allan, An adaptive weighted median filter for speckle suppression in medical ultrasonic images. *Circuits and Systems, IEEE Transactions on*, Vol.36, No.1, 1989. pp. 129-135.
[34] Lai Khin Wee, Hum Yan Chai, Eko Supriyanto, Surface rendering of three dimensional ultrasound images using VTK,

Journal of Scientific & Industrial Research, Vol. 70, 2011, pp. 421-426.

[35] Wee L.K., Eko S., Automatic Detection of Fetal Nasal Bone in 2 Dimensional Ultrasound Image Using Map Matching, *12th WSEAS International Conference on Automatic Control, Modeling & Simulation*, 2010, pp. 305-309.

[36] Eko S., Wee L.K., Min T.Y., Ultrasonic Marker Pattern Recognition and Measurement Using *Artificial Neural Network, 9th WSEAS International Conference on Signal Processing*, 2010, pp. 35-40.

[37] Wee L.K., Arroj A., Eko S., Computerized Automatic Nasal Bone Detection based on Ultrasound Fetal Images Using Cross Correlation Techniques, *WSEAS Transactions on Information Science and Applications*, Vol. 7, No. 8, 2010, pp. 1068-1077.

[38] Wee L.K., et al., Nuchal Translucency Marker Detection Based on Artificial Neural Network and Measurement via Bidirectional Iteration Forward Propagation, *WSEAS Transactions on Information Science and Applications*, Vol.7, No.8, pp. 1025-1036.